

# Clustering of gyrotactic microorganisms in turbulent flows

Filippo De Lillo,<sup>1,2</sup> Guido Boffetta,<sup>2</sup> and Massimo Cencini<sup>3</sup>

<sup>1</sup>*Dipartimento di Ingegneria delle Costruzioni, dell'Ambiente e del Territorio, Università di Genova, via Montallegro 1, 16145 Genova, Italy*

<sup>2</sup>*Dipartimento di Fisica and INFN, Università di Torino, via P. Giuria 1, 10125 Torino, Italy*

<sup>3</sup>*Istituto dei Sistemi Complessi, Consiglio Nazionale delle Ricerche, via dei Taurini 19, 00185 Rome, Italy*

We study the spatial distribution of gyrotactic microorganisms transported by a three-dimensional turbulent flow generated by direct numerical simulations. We find that gyrotaxis combines with turbulent fluctuations to produce small scales (multi-)fractal clustering. We explain this result by showing that gyrotactic swimming cells behave like tracers in a compressible flow. The effective compressibility is derived in the limits of fluid acceleration much larger and smaller than the gravity.

PACS numbers: 05.45.-a, 47.63.Gd, 92.20.jf

Microbial patchiness in oceans is important for ecological and evolutionary dynamics [1, 2] and for biogeochemical processes [3]. In motile aquatic microorganisms, self-propulsion provides a mechanism to escape fluid pathlines, potentially leading to small-scale patchiness [4–6]. Remarkably, motility combined with fluid flows can also generate large-scale inhomogeneities. For instance, spectacular aggregation of phytoplankton cells (in layers centimeters to meters thin, horizontally extending from hundreds of meters to kilometers) can result from vertical shears and *gyrotactic swimming* [7]. Gyrotaxis characterizes several species of motile microalgae whose swimming direction is determined by the balance of viscous and gravitational torques, due to the displacement between the cell center of mass and buoyancy. As an effect of such balance, for example, gyrotactic algae aggregate in the center (wall) of descending (ascending) vertical pipe flows [8, 9]. Gyrotaxis is observed in algae, e.g., of the genus *Chlamydomonas*, which can be engineered to transport microloads [10], or *Dunaliella*, employed in bio-fuels [11]. So far most studies focused on the dynamics of gyrotactic microorganisms in simple stationary flows or kinematic models [6–9, 12, 13].

In this Letter, we investigate the interplay between gyrotactic motility and realistic turbulent flows, as occurring in the sea. We find that turbulence and gyrotaxis combine to generate inhomogeneous distributions with small-scale (multi-)fractal statistics (see Fig. 1). We study the limit of gravitational acceleration much smaller or larger than turbulent accelerations to identify the mechanisms responsible for gyrotactic clustering in terms of an effective compressible velocity field.

We consider dilute suspensions of non interacting motile microorganisms, much smaller than the smallest scale of turbulence, the Kolmogorov length  $\eta$ . We can thus model them as self-propelled particles with velocity,

$$\dot{\mathbf{X}} = \mathbf{u}(\mathbf{X}, t) + v_s \mathbf{p}, \quad (1)$$

given by the sum of the fluid velocity  $\mathbf{u}$  at the particle position  $\mathbf{X}$  and the swimming contribution  $v_s \mathbf{p}$ , where the swimming speed  $v_s$  is assumed constant [5, 9]. Cells

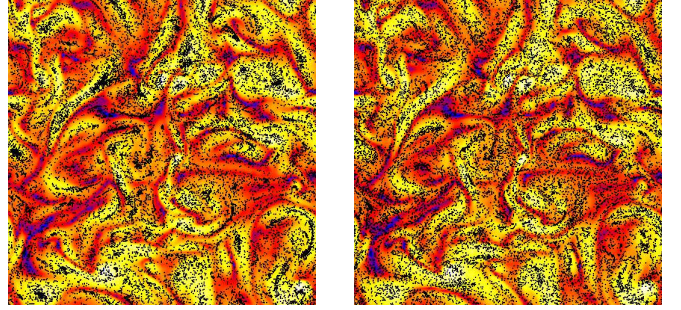


FIG. 1. (color online) Spatial distribution of gyrotactic swimmers (dots) in a slab of a 3D turbulent flow. Color code: yellow/blue corresponds to high/low vorticity values ( $\ln|\boldsymbol{\omega}|/\omega_{\text{rms}}$ ). (Left) Limit of orientation dominated by local fluid acceleration ( $\mathbf{A} = \mathbf{a}$ , see text) with aggregation in high vorticity regions. (Right) Limit of gravity dominated orientation ( $\mathbf{A} = -\mathbf{g}$ ). Parameters correspond to circled symbols in Fig. 2c and Fig. 3a, respectively.

are assumed spherical and neutrally buoyant, with the center of mass displaced by  $h$  with respect to the geometric one. The swimming direction  $\mathbf{p}$ , determined by the total torque acting on the cell, evolves as

$$\dot{\mathbf{p}} = \frac{1}{2v_o} [\mathbf{A} - (\mathbf{A} \cdot \mathbf{p})\mathbf{p}] + \frac{1}{2}\boldsymbol{\omega} \times \mathbf{p}, \quad (2)$$

where  $\boldsymbol{\omega}$  is the fluid vorticity and  $v_o = 3\nu/h$  is the orientation speed for spherical cells subject to the acceleration  $\mathbf{A}$  [9]. In a fluid at rest, besides viscous forces, only gravity (and buoyancy)  $\mathbf{g}$  is acting and thus  $\mathbf{A} = -\mathbf{g} = g\hat{\mathbf{z}}$ , while acceleration due to swimming is neglected [9]. In presence of a flow, we have  $\mathbf{A} = \mathbf{a} - \mathbf{g}$  where

$$\mathbf{a} \equiv \partial_t \mathbf{u} + \mathbf{u} \cdot \nabla \mathbf{u} = -\nabla p + \nu \nabla^2 \mathbf{u} + \mathbf{f} \quad (3)$$

is the fluid acceleration given by the Navier-Stokes equations ruling the velocity  $\mathbf{u}$  of an incompressible ( $\nabla \cdot \mathbf{u} = 0$ ) fluid with viscosity  $\nu$ , pressure  $p$  and stirred by an external forcing  $\mathbf{f}$ . Previous studies on gyrotactic swimmers disregarded fluid acceleration, as mainly focused on simple, non-turbulent flows where  $|\mathbf{a}| \ll g$ . In tur-

bulence, fluid acceleration can locally exceed  $g$  [14] and therefore its contribution has to be taken into account.

The first term on the rhs of Eq. (2) causes the direction of swimming  $\mathbf{p}$  to align with  $\mathbf{A}$  on a time scale  $v_o/A$ . When the contribution of fluid acceleration can be neglected, cells tend to orient vertically ( $\mathbf{p} \rightarrow \hat{\mathbf{z}}$ ) on a time scale  $B = v_o/g$ . The alignment is contrasted by the vorticity term  $\boldsymbol{\omega} \times \mathbf{p}$  and, depending on  $B\omega$  being smaller or larger than 1, cells may swim along a resulting local equilibrium direction or tumble randomly as the orientation becomes unstable due to vorticity [9, 13]. In principle, the swimming direction may be modified also by rotational Brownian motion [15] and tumbling due to flagella desynchronization during swimming [16], which are here neglected. The former effect is very small for typical algae (having size  $\mathcal{O}(10\mu\text{m})$ ); the latter can be neglected whenever the tumbling time is longer than the reorientation one.

We study gyrotactic swimming in homogeneous and isotropic turbulent velocity fields of moderate intensity ( $Re_\lambda \approx 65 - 100$ ) by means of direct numerical simulations of Navier-Stokes equations. In particular, Eq. (3) is solved by means of a standard pseudospectral algorithm with  $2^{nd}$  order Runge-Kutta time-stepping, on a tri-periodic cubic grid of size  $N^3$  (for  $N=128$  and  $256$ ). Statistical stationarity is guaranteed by means of a zero mean, Gaussian and white in time random forcing  $\mathbf{f}$  restricted to large scales. Viscosity  $\nu$  is such that the Kolmogorov length  $\eta$  is of the order of the grid spacing, ensuring well resolved small-scale velocity dynamics. For different values of  $g$ , several populations of swimmers, characterized by different values of  $v_s$  and  $v_o$  are injected with random positions and orientations. At each time step, velocity and acceleration at the swimmers positions, needed to integrate Eqs. (1-2), are obtained by interpolation. The self-propelled particles are then evolved, and their distribution and orientation studied in statistically steady conditions. In the sequel, we mostly focus on the dependence on the orientation speed  $v_o$  by fixing  $v_s \approx 0.3u_\eta$ ,  $u_\eta$  being the typical fluid velocity fluctuation at the Kolmogorov scale.

Formally, Eqs. (1-2) define a dissipative dynamical system evolving in the  $2d$ -dimensional (actually  $2d-1$  because  $\mathbf{p}^2=1$  and  $d=3$ ) phase space  $(\mathbf{X}, \mathbf{p})$  with phase-space contraction rate

$$\Gamma = \sum_{i=1}^d \frac{\partial \dot{X}_i}{\partial X_i} + \sum_{i=1}^d \frac{\partial \dot{p}_i}{\partial p_i} = -\frac{d+1}{2v_o} (gp_z + \mathbf{a} \cdot \mathbf{p}). \quad (4)$$

As  $\mathbf{p}$  orients in the direction  $\mathbf{a} - \mathbf{g}$ ,  $\Gamma$  is expected to be negative on average, meaning that swimmers will evolve onto a dynamical attractor of dimension smaller than the whole phase space, which explains why clustering can be observed: if the fractal dimension of the attractor is smaller than  $d$ , clustering in position space (as in Fig. 1) is possible (see Ref. [17] for a conceptually similar phe-

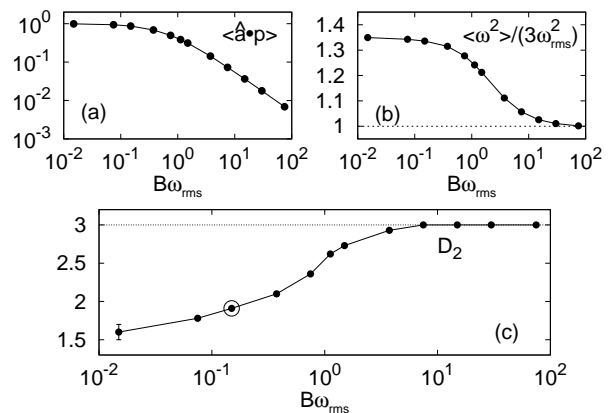


FIG. 2. Swimmer properties as a function of the orientation parameter  $B\omega_{rms}$  ( $B = v_o/a_{rms}$ ) in the limit  $|\mathbf{a}| \gg g$ . (a) Average alignment with fluid acceleration  $\langle \hat{\mathbf{a}} \cdot \mathbf{p} \rangle$ . (b) Average square vorticity at swimmers position normalized to the volume average value. (c) correlation dimension  $D_2$ . Circled symbol in (c) corresponds to the distribution shown in Fig. 1a.

nomenon occurring for inertial particles). We remark that clustering is a consequence of swimming: indeed for  $v_s = 0$  Eqs. (1) and (2) decouple, thus cells become tracers advected by an incompressible velocity and cannot cluster. Moreover, in the limit  $v_o \rightarrow \infty$  we have  $\Gamma \rightarrow 0$  and therefore swimmers cannot cluster. Nonetheless, even in this limit, if  $v_s > 0$  they deviate from fluid trajectories and generate interesting dynamics [18].

We now discuss the physical mechanisms of clustering which, as anticipated, depend on whether the dominating effect comes from the gravitational ( $g$ ) or fluid acceleration (which we quantify in terms of its rms value  $a_{rms}$ ).

We start considering the case  $a_{rms} \gg g$  and therefore we take  $\mathbf{A} = \mathbf{a}$  in Eq. (2). Figure 2 summarizes the behavior of the main observables as a function of the dimensionless number  $B\omega_{rms}$  (now  $B = v_o/a_{rms}$ ) measuring the ratio of the alignment timescale to rotation timescale induced by vorticity. When the alignment is very fast, the swimming direction  $\mathbf{p}$  becomes parallel to the local direction of the fluid acceleration  $\hat{\mathbf{a}} = \mathbf{a}/a$ , as confirmed by Fig. 2a showing that  $\langle \hat{\mathbf{a}} \cdot \mathbf{p} \rangle \rightarrow 1$  for  $B\omega_{rms} \ll 1$  (here and in the following  $\langle [\cdot] \rangle$  denotes average over particle distribution). In this limit, swimming cells behave like tracers advected by an effective velocity  $\mathbf{v} \approx \mathbf{u} + v_s \hat{\mathbf{a}}$ . While  $\mathbf{u}$  is incompressible, the effective velocity field  $\mathbf{v}$  is not:  $\nabla \cdot \mathbf{v} \propto v_s \nabla \cdot \mathbf{a}$  being negative (positive) in high vorticity (strain) regions. Therefore, as it occurs for inertial particles lighter than fluid [19, 20], the swimmers cluster inside vortical structures (Fig. 1a and Fig. 2b). The divergence of  $\mathbf{v}$  is proportional to  $v_s$ , clustering is thus expected to increase with the swimming speed. In the opposite limit of slow alignment, when  $B\omega_{rms} \gg 1$ , random tumbling due to fluid vorticity dominates, hence swimming orientation cannot align to the local acceleration ( $\langle \hat{\mathbf{a}} \cdot \mathbf{p} \rangle \rightarrow 0$ , see Fig. 2a): the compressible effect is

lost and particles distribute uniformly in the volume. To quantify clustering we measured the correlation dimension  $D_2$ , ruling the small-distance ( $r \rightarrow 0$ ) behavior of the probability to find two swimmers at separation less than  $r$ :  $P_2(|\mathbf{X}_1 - \mathbf{X}_2| < r) \propto r^{D_2}$  [21]. For uniformly distributed particles  $D_2 = d$ , while when clustering is present the probability to find close pairs increases and  $D_2 < d$  (see e.g. [22] for a similar study in the case of inertial particles). In Fig. 2c we show  $D_2$  as a function of  $B\omega_{\text{rms}}$ : for  $B\omega_{\text{rms}} \ll 1$ ,  $D_2 \approx 1.5$ , indicating strong clustering in almost filamental structures; conversely, when  $B\omega_{\text{rms}} > 1$ , the correlation dimension approaches the uniform-distribution value  $D_2 \approx 3$ .

We now consider the limit  $a_{\text{rms}} \ll g$  when we can take  $\mathbf{A} = -\mathbf{g}$  and Eq. (2) reads

$$\dot{\mathbf{p}} = \frac{1}{2B}(\hat{\mathbf{z}} - p_z \mathbf{p}) + \frac{1}{2}\boldsymbol{\omega} \times \mathbf{p}, \quad (5)$$

with  $B = v_o/g$ . Similarly to the previous case, when  $B\omega_{\text{rms}} \rightarrow 0$  the cells orient in the preferred direction  $\hat{\mathbf{z}}$ , which is now fixed in space. The effective velocity thus becomes  $\mathbf{v} = \mathbf{u} + v_s \hat{\mathbf{z}}$  which, unlike the previous case, is incompressible ( $\nabla \cdot \mathbf{v} = 0$ ). Therefore, now we expect that not only for  $B\omega_{\text{rms}} \gg 1$  but also for  $B\omega_{\text{rms}} \rightarrow 0$  swimmers distribute uniformly, as confirmed by Fig. 3a showing that  $D_2 \rightarrow 3$  in both limits. Remarkably, Fig. 3a shows that also in this case gyrotactic swimmers cluster on a fractal set (see Fig. 1b) for intermediate values, with a well defined minimum of the correlation dimension ( $D_2 \approx 2.7$ ) for  $B\omega_{\text{rms}} \sim \mathcal{O}(1)$ . We remark that an optimal orientation timescale for aggregation is also observed in steady kinematic vortical flows [6] where, however, a vast class of trajectories is integrable.

We can understand the origin of the observed clustering by considering the limit  $B\omega_{\text{rms}} \ll 1$ . In such limit, cell orientation being very fast we can assume that the swimming direction  $\mathbf{p}$  is always at an equilibrium orientation with  $p_x, p_y \ll p_z \simeq 1$  (see Fig. 3b). In particular,

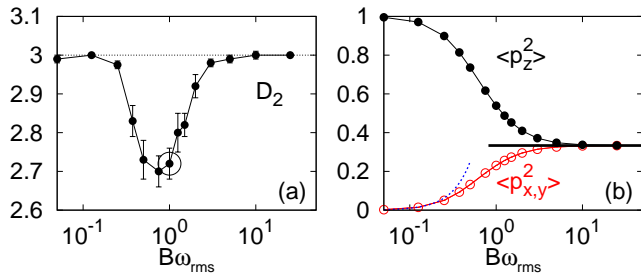


FIG. 3. (color online) Clustering properties as a function of  $B\omega_{\text{rms}}$ , for  $g \gg |a|$  ( $B = v_o/g$ ). (a) Correlation dimension  $D_2$  of the swimmer positions. Circled symbol corresponds to the data shown in Fig. 1b. (b) Variances of swimming direction components ( $\langle p_x^2 \rangle = \langle p_y^2 \rangle$  in red, and  $\langle p_z^2 \rangle$ ). The dashed blue curve is the parabola  $(B\omega_{\text{rms}})^2$ . The solid horizontal line represents the random orientation value  $1/3$ .

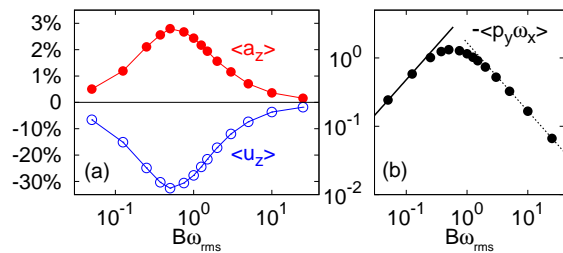


FIG. 4. (color online) (a) Average fluid acceleration (positive, red filled circles) and velocity (negative, blue open circles) along the vertical at swimmer positions, expressed in percentage of  $a_{\text{rms}}$  and  $v_s$ , respectively. (b) Correlation  $-\langle p_y \omega_x \rangle$  vs  $B\omega_{\text{rms}}$ . The maximum for  $B\omega_{\text{rms}} \sim \mathcal{O}(1)$  is understood noticing that  $-\langle p_y \omega_x \rangle$  must decrease for  $B\omega_{\text{rms}} \gg 1$ . In the limit  $B\omega_{\text{rms}} \ll 1$ ,  $-\langle p_y \omega_x \rangle \simeq B\omega_{\text{rms}}^2$  (solid line) is implied by  $\mathbf{p} \simeq (B\omega_x, -B\omega_y, 1)$ , see text. In the random tumbling limit  $\langle p_x^2 \rangle = \langle p_y^2 \rangle \rightarrow 1/3$  (Fig. 3a), which implies  $-\langle p_y \omega_x \rangle = \langle p_y^2 \rangle_s / B \sim 1/(3B)$  (dashed line).

solving Eq. (5) for  $\dot{\mathbf{p}} = 0$ , at first order in  $p_x, p_y$ , one finds  $p_x \simeq B\omega_y$  and  $p_y \simeq -B\omega_x$  (which is confirmed by simulations). As a consequence, the effective swimmer velocity field  $\mathbf{v} = \mathbf{u} + v_s \mathbf{p}$  with  $\mathbf{p} \simeq (B\omega_y, -B\omega_x, 1)$  has a compressible component with divergence

$$\nabla \cdot \mathbf{v} \simeq -v_s B \nabla^2 u_z, \quad (6)$$

which, unlike the previous case, is unrelated to fluid acceleration so that swimmers will cluster in regions different from those of high vorticity (compare Fig. 1a and b). We notice that (6) generalizes the well known mechanism of cell focusing in the center (walls) of downward (upward) vertical pipe flows [8]. Notice that in the above argument the vertical component of the vorticity plays no role, as it does not change  $p_z$ .

Another consequence of the expansion  $\mathbf{p} \simeq (B\omega_x, -B\omega_y, 1)$  is that  $p_x$  (resp.  $p_y$ ) and  $\omega_y$  ( $\omega_x$ ) have locally the same (opposite) sign. Numerical simulations show that this remains true also for larger values of  $B\omega_{\text{rms}}$ , on average. Indeed, at stationarity, by averaging Eq. (5) and using isotropy on the  $(x, y)$  plane (guaranteed by the isotropy of the fluid velocity field) we obtain  $\langle p_x^2 \rangle = \langle p_y^2 \rangle = B \langle p_x \omega_y \rangle = -B \langle p_y \omega_x \rangle$ . The correlation between the horizontal components of  $\mathbf{p}$  and  $\boldsymbol{\omega}$  implies that the swimmers will stay longer in regions of the flow characterized by positive vertical velocity and negative vertical acceleration (Fig. 4a). This can be easily seen in a case with, say, a vortex aligned with the  $x$ -axis, where the above argument with  $\omega_x > 0$  implies  $\langle p_z \rangle > 0$ ,  $\langle p_y \rangle < 0$ , so that the trajectories spend more time in regions where  $a_z > 0, u_z < 0$  as there the swimming velocity opposes that of the fluid. The preferential concentration in these regions of the flow will be maximal (and correspondingly the correlation dimension minimal, i.e. clustering stronger) for  $B\omega_{\text{rms}} \sim \mathcal{O}(1)$  where the correlation between swimming direction and vorticity



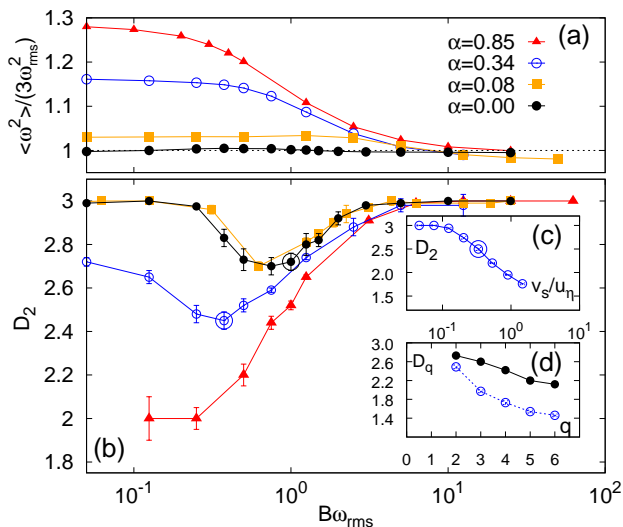


FIG. 5. (color online) (a) Average square vorticity at swimmers position normalized to the volume average value at varying the ratio  $\alpha = a_{rms}/g$  ( $\alpha = 0$  corresponds to data of Fig. 3); (b) correlation dimension  $D_2$  vs  $\alpha$ ; (c)  $D_2$  vs swimming speed  $v_s/u_\eta$ , the circled symbol corresponds to the circled one in (b); (d) generalized dimensions  $D_q$  vs  $q$  for circled data in (b), notice that the case  $\alpha = 0$  (filled black circles) appears to be less multifractal than when also the fluid acceleration is contributing to clustering (empty blue circles).

$-\langle p_y \omega_x \rangle = \langle p_x \omega_y \rangle$  is also maximal (Fig. 4b). For such value of  $B\omega_{rms}$  fluid regions with maximal deviation of the swimming direction from the vertical will balance vorticity dominated ones where  $\mathbf{p}$  tumbles randomly. We observe that the swimmer vertical migration can be strongly inhibited by the bias towards downwelling regions: in Fig. 4a, e.g.,  $\langle u_z \rangle$  can reach 30% of the swimming speed  $v_s$ .

In the general case, the relative importance of fluid and gravitational accelerations for clustering depends on the ratio  $\alpha = a_{rms}/g$ . Figure 5a indeed shows that the bias towards regions of high vorticity decreases with  $\alpha$  and is absent when only the gravitational torque is acting ( $\alpha = 0$ ). The correlation dimension  $D_2$ , shown in Fig. 5b, smoothly varies with  $\alpha$ , interpolating from the two limits shown in Fig. 2c and 3b. We observe that, as anticipated, clustering is more effective for large swimming speeds as displayed in Fig. 5c, showing that, at fixed value of  $B\omega_{rms}$ ,  $D_2$  decreases with  $v_s/u_\eta$ . Finally, as one can expect from general considerations on dynamical attractors [17], Fig. 5d demonstrates that the spatial distribution of the gyrotactic self-propelled particles is multifractal, as the generalized dimensions  $D_q$  (controlling the probability to find  $q$  particles at small separation) depends on the moment  $q$  [21].

Summarizing, we have shown that gyrotactic motility and realistic turbulent flows can generate small-scale patchiness (down to the Kolmogorov scale) in the distribution of bottom-heavy swimming microorganisms. We

identified two mechanisms driving microorganism clustering: the focusing in vortical regions due to local adjustment of the swimming orientation with fluid acceleration, and the correlation between vorticity and swimming direction on the plane perpendicular to gravity leading particles to preferentially explore downwelling, upward accelerating regions. In general, gravity is expected to dominate when turbulent intensity is not very high and it is likely the most important effect in the ocean. Crucial parameters for observing clustering are in this case the ratio between swimming speed and small-scale fluid velocity fluctuations ( $v_s/u_\eta$ ) and the reorientation time scale with respect to vorticity intensity ( $B\omega_{rms}$ ). For typical microalgae  $B \approx 1 - 6s$  and  $v_s = 100 - 200 \mu m/s$  [8, 23, 24]. In the ocean, the turbulence intensity, measured in terms of kinetic energy dissipation  $\epsilon$ , varies from  $\epsilon \sim 10^{-4} - 10^{-5} W/Kg$  in the upper mixing layer down to  $\epsilon \sim 10^{-6} - 10^{-7} W/Kg$  a few meters deeper [25, 26]. We can thus estimate that  $v_s/u_\eta \in [0.02 : 0.4]$  and  $B\omega_{rms} \in [0.1 : 50]$  therefore the effects discussed in this Letter are relevant in realistic conditions and can definitely be tested in laboratory by tuning turbulence characteristics.

We conclude by remarking that for non-spherical cells such as, e.g., prolate spheroids the term  $\gamma \mathbf{p} \cdot \mathbb{S} \cdot (\mathbb{I} - \mathbf{p} \otimes \mathbf{p})$  should be added to Eq. (2) ( $\gamma$  being the eccentricity, and  $\mathbb{S}$  and  $\mathbb{I}$  the symmetric rate of strain tensor and identity matrix, resp.) [9]. Such term is also contributing to the phase-space contraction rate (4) providing an additional mechanism for clustering [5]. It will thus be interesting to study if and how gyrotactic clustering in turbulence is modified at varying the cell shape.

We thanks S. Musacchio for useful discussions. GB and MC acknowledge KITPC institute for hospitality during the program *New Directions in Turbulence* and support by MIUR PRIN-2009PYYZM5 “Fluttuazioni: dai sistemi macroscopici alle nanoscale”.

- 
- [1] S. Levin and M. Whitfield, *Philos. T. Roy. Soc. B* **343**, 99 (1994).
  - [2] F. Azam and F. Malfatti, *Nat. Rev. Microbiol.* **5**, 782 (2007).
  - [3] P. Falkowski *et al.*, *Science* **290**, 291 (2000).
  - [4] J. Mitchell, A. Okubo, and J. Fuhrman, *Limn. Ocean.* **35**, 123 (1990).
  - [5] C. Torney and Z. Neufeld, *Phys. Rev. Lett.* **99**, 078101 (2007).
  - [6] W. Durham, E. Climent, and R. Stocker, *Phys. Rev. Lett.* **106**, 238102 (2011).
  - [7] W. M. Durham, J. O. Kessler, and R. Stocker, *Science* **323**, 1067 (2009).
  - [8] J. O. Kessler, *Nature* **313**, 218 (1985).
  - [9] T. J. Pedley and J. O. Kessler, *Proc. Royal Soc. B* **231**, 47 (1987); *Annu. Rev. Fluid Mech.* **24**, 313 (1992).
  - [10] D. Weibel *et al.*, *Proc. Natl. Acad. Sci. USA* **102**, 11963

- (2005).
- [11] Y. Chisti, *Biotech. Advances* **25**, 294 (2007).
- [12] N. A. Hill and M. A. Bees, *Phys. Fluids* **14**, 2598 (2002).
- [13] G. J. Thorn and R. N. Bearon, *Phys. Fluids* **22**, 041902 (2010).
- [14] A. La Porta *et al.*, *Nature* **409**, 1017 (2001).
- [15] H. Berg, *Random walks in biology* (Princeton Univ Pr, 1993).
- [16] M. Polin *et al.*, *Science* **325**, 487 (2009).
- [17] J. Bec, *J. Fluid Mech.* **528**, 255 (2005).
- [18] N. Khurana, J. Blawdziewicz, and N. T. Ouellette, *Phys. Rev. Lett.* **106**, 198104 (2011).
- [19] E. Balkovsky, G. Falkovich, and A. Fouxon, *Phys. Rev. Lett.* **86**, 2790 (2001).
- [20] E. Calzavarini *et al.*, *Phys. Rev. Lett.* **101**, 84504 (2008).
- [21] G. Paladin and A. Vulpiani, *Phys. Rep.* **156**, 147 (1987).
- [22] J. Bec *et al.*, *Phys. Rev. Lett.* **98**, 84502 (2007).
- [23] M. S. Jones, L. Le Baron, and T. J. Pedley, *J. Fluid Mech.* **281**, 137 (1994).
- [24] N. Hill and D. Häder, *J. Theor. Biol.* **186**, 503 (1997).
- [25] H. Yamazaki and K. Squires, *Mar. Ecol. Prog. Ser.* **144**, 299 (1996).
- [26] H. Yamazaki, D. L. Mackas, and K. L. Denman, in *The sea: biological-physical interaction in the ocean*, Vol. 12 (John Wiley & Sons, New York, 2002) p. 51.